Penta-MP_5 (M=B, Al, Ga, In) Monolayers as High-Performance Photocatalysts for Overall Water Splitting

Jiao Chen,[1] Xinyong Cai,[1,] * Xiaotao Zhang,[1] Hongyan Wang,[1,] * Yuxiang Ni,[1] Xuefei Liu,[2] Yuanzheng Chen [a,] *

[1] *School of Physical Science and Technology, Key Laboratory of Advanced Technologies of Materials, Ministry of Education of China, Southwest Jiaotong University, Chengdu 610031, China.*
[2] *School of Physical and Electronic Sciences, Guizhou Normal University, Guiyang 550025, China.*

**E-mail:* cyz@swjtu.edu.cn, (X. C.) caixinyong@my.swjtu.edu.cn and (Y.H.) hongyanw@swjtu.edu.cn

Table of Contents for Supporting Information

Structures and stabilities of Penta-MP_5 monolayers

Table S1. The lattice constants ($a = b$) and thickness (h) of the sheet of Penta-MP_5 (M= B, Al, Ga, and In) monolayers and previous work are in brackets.

Penta-MP_5 (M = B, Al, Ga, and In)	$a = b$ (Å)	h (Å)
Penta-BP_5	4.54 (4.54[1])	2.51
Penta-AlP_5	4.89 (4.89[2])	2.63
Penta-GeP_5	4.91 (4.92[2])	2.80
Penta-InP_5	5.06 (5.06[2])	2.93

Table S2. The cohesive energy of Penta-MP_5 (M = B, Al, Ga, and In) monolayers and previous work are in brackets.

Penta-MP_5 (M = B, Al, Ga, and In)	Cohesive energy (eV/atom)	
	Our results	Previous works
Penta-BP_5	-4.68[1]	
Penta-AlP_5	-4.54[2]	-4.54[2]
Penta-GeP_5	-4.37[2]	-4.37[2]
Penta-InP_5	-4.22[2]	-4.21[2]

Table S3. The Calculated in-plane stiffeness constants C_{mn} of Penta-MP_5 monolayers.

Penta-MP_5 (M = B, Al, Ga, and In)	$C_{11} = C_{22}$	C_{12}	C_{66}
Penta-BP_5	72.86	13.62	52.25
Penta-AlP_5	56.70	10.40	28.19
Penta-GaP_5	56.78	11.37	29.79
Penta-InP_5	48.60	11.24	22.91

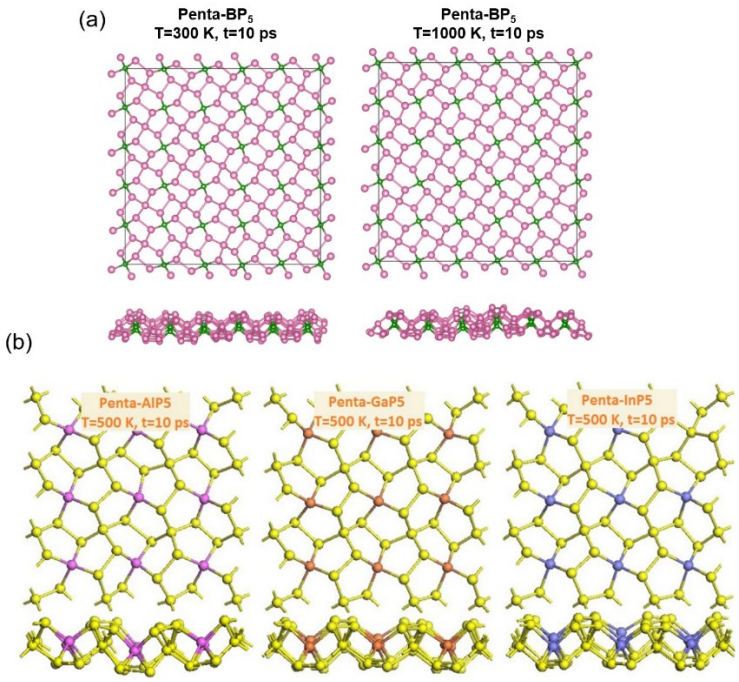

Figure S1. (a) Top and side views of the penta-BP_5 monolayer structures at 300 K and 1000 K after 10 ps in the AIMD simulations.[1] (b) Top and side views of the penta-AlP_5, penta-GaP_5, penta-InP_5 monolayer structures at 500 K after 10 ps in the AIMD simulations.[2]

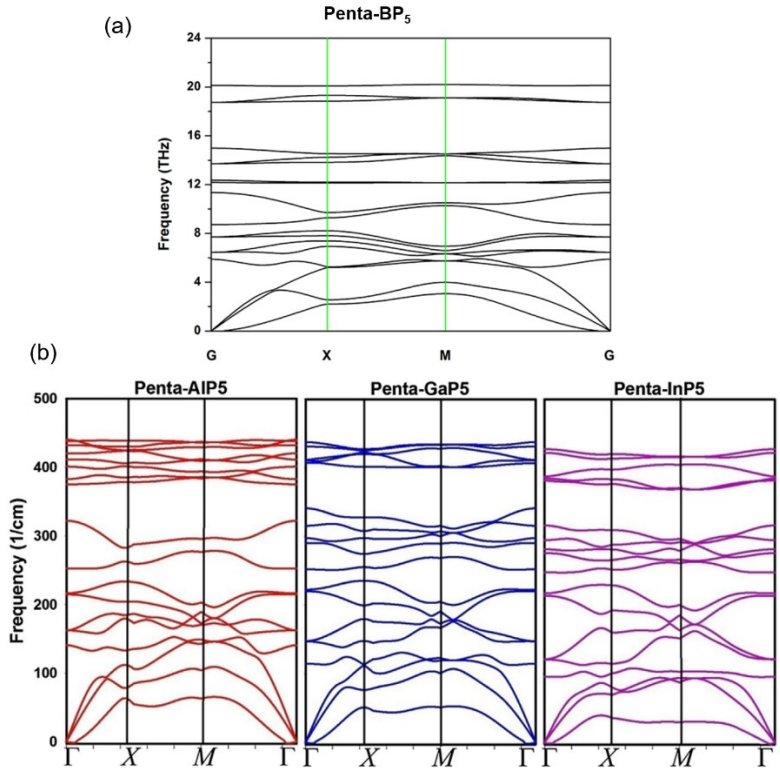

Figure S2. (a) the calculated phonon dispersion of Penta-BP_5 monolayers.[1] (b) the calculated phonon dispersion of Penta-AlP_5, Penta-GaP_5, Penta-InP_5 monolayers.[2]

Electronic structures of Penta-MP_5 monolayers for water splitting

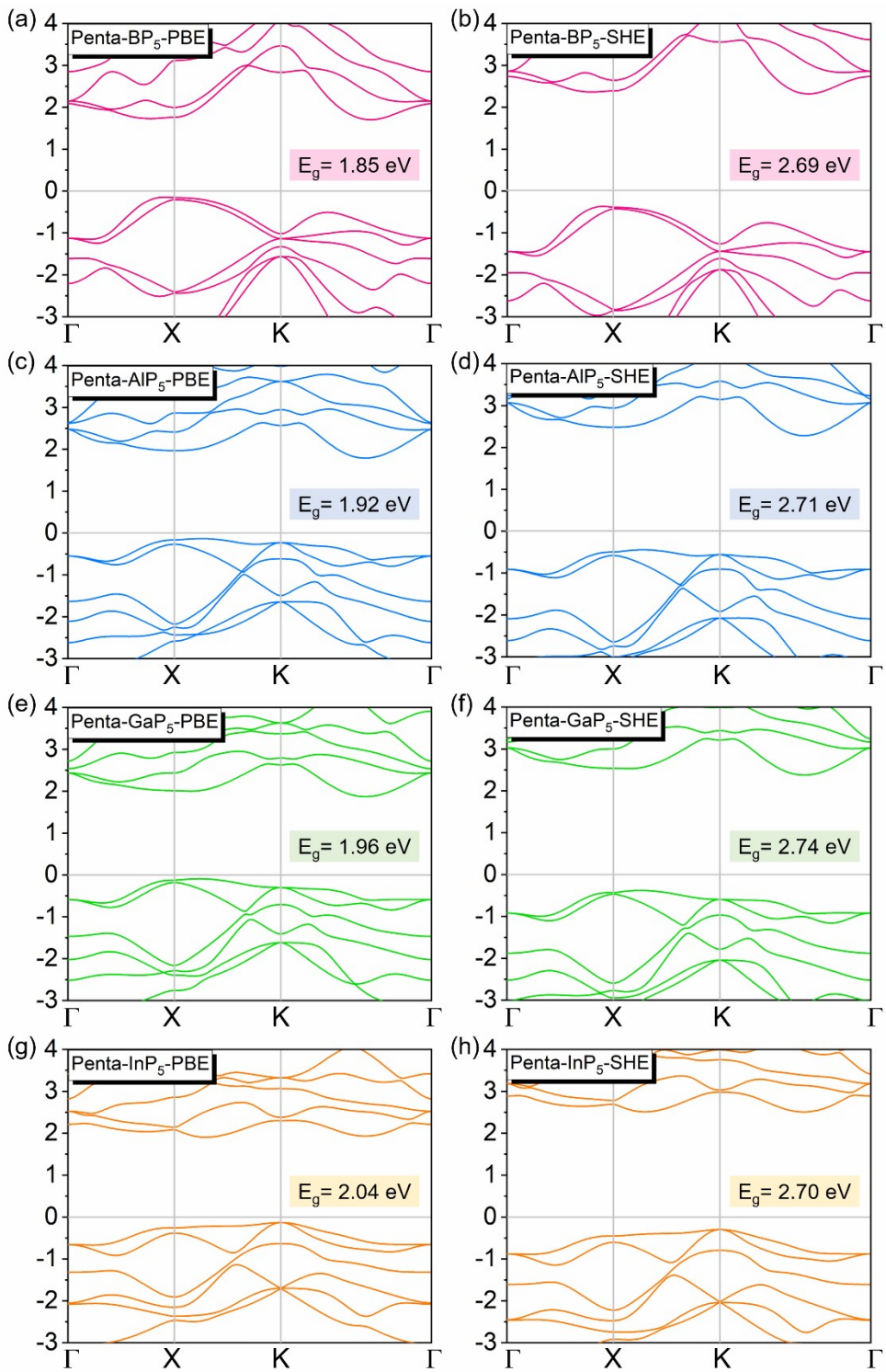

Figure S3. The calculated band structures of Penta-MP_5 monolayers relative to the Fermi level in the first Brillouin zone along the path (Γ-X-K-Γ) by the PBE method and hybrid functional method HSE06.

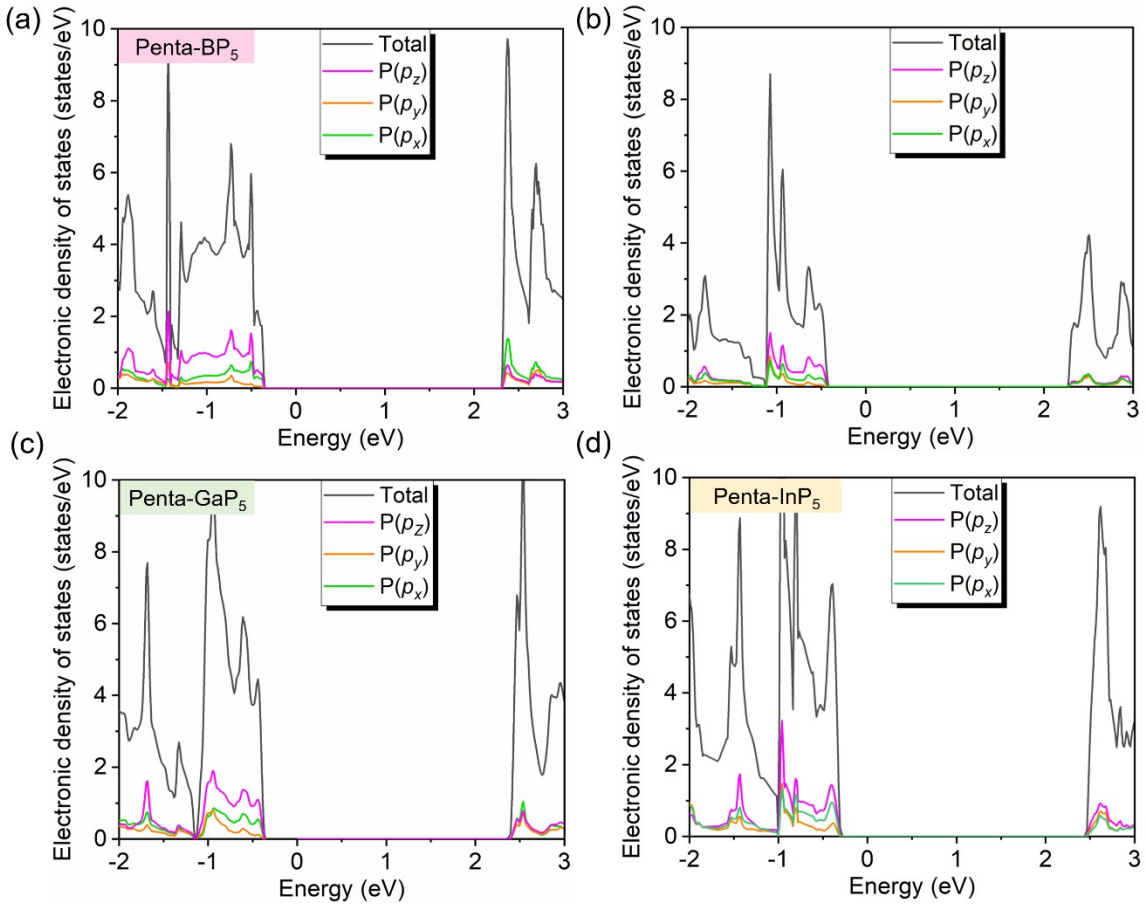

Figure S4. The calculated partial DOS of Penta-MP_5 monolayers.

Stable stacking patterns of bilayer Penta-MP_5

The most feasible stacking patterns of bilayer Penta-MP_5, named AA, AB, and AC, are initially considered. As depicted in Figure S5 (a), the AA pattern denotes the overlapping schema, i.e., the upper M atoms are positioned directly overhead the lower M atoms. The AB pattern and AC pattern are constructed by staggered stacking, where the upper layer in the AA pattern is translated with respect to the lower layer. In the AB pattern and AC pattern, the tri-coordinated P atoms and tetra-coordinated P atoms in the upper layer are shifted above the M atoms in the lower layer, respectively, as shown in Figure S5 (b)-(c). After undergoing complete structural optimization, the AB mode is found to be relaxed to the AA pattern. Therefore, we ignore the AB pattern and only consider the AA pattern and AC pattern in the following discussion. By calculating their total energies, we find AA pattern have lower total energies than AC pattern as listed in Table S4. Hence, the AA pattern is more stable than AC pattern.

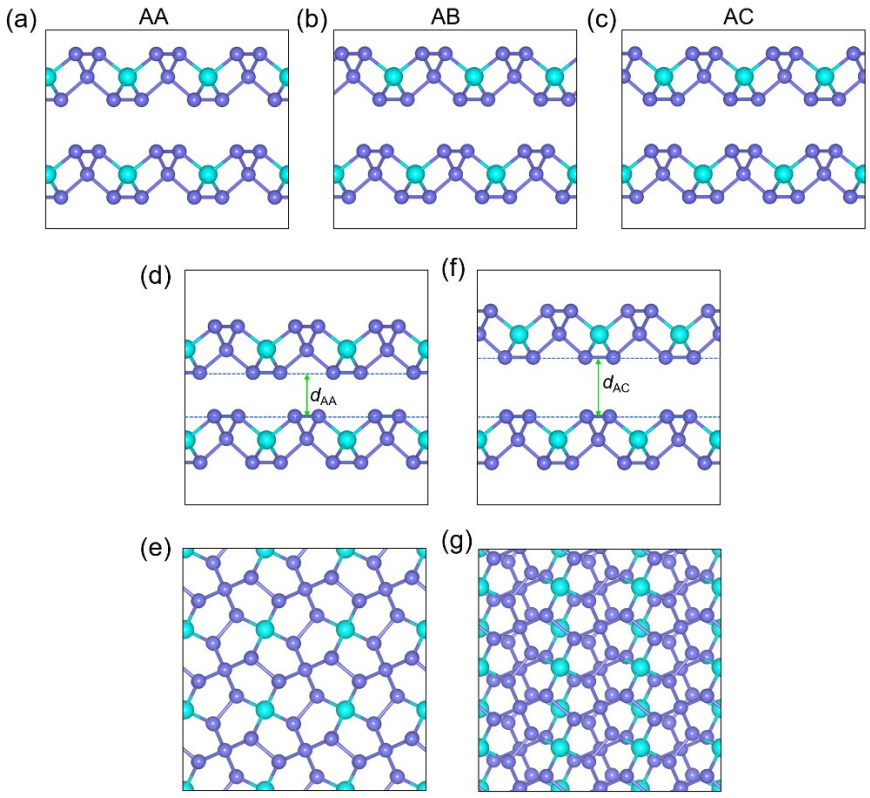

Figure S5. The structural models of bilayer Penta-MP_5 stacked in (a) AA pattern, (b) AB pattern and (c) AC pattern. The side (d) and top (e) views of the optimized crystal structures of bilayer Penta-MP_5 stacked in AA and AB. The side (f) and top (g) views of the optimized crystal structures of bilayer Penta-MP_5 stacked in AC.

Table S4. The interlayer distance *d* (Å), total energies E (eV/atom) and bandgap E_g(eV) (in PBE level) of bilayer Penta-MP_5 in AA pattern and AC pattern.

Penta-MP_5	AA			AC		
(M = B, Al, Ga, and In)	*d* (Å)	E (eV/atom)	E_g(eV)	*d* (Å)	E (eV/atom)	E_g(eV)
Penta-BP_5	2.65	-5.33	1.45	3.57	-5.31	1.58
Penta-AlP_5	2.41	-5.75	1.59	3.81	-5.72	1.61
Penta-GeP_5	2.46	-5.18	1.43	3.60	-5.16	1.62
Penta-InP_5	2.60	-5.03	1.54	3.45	-5.02	1.73

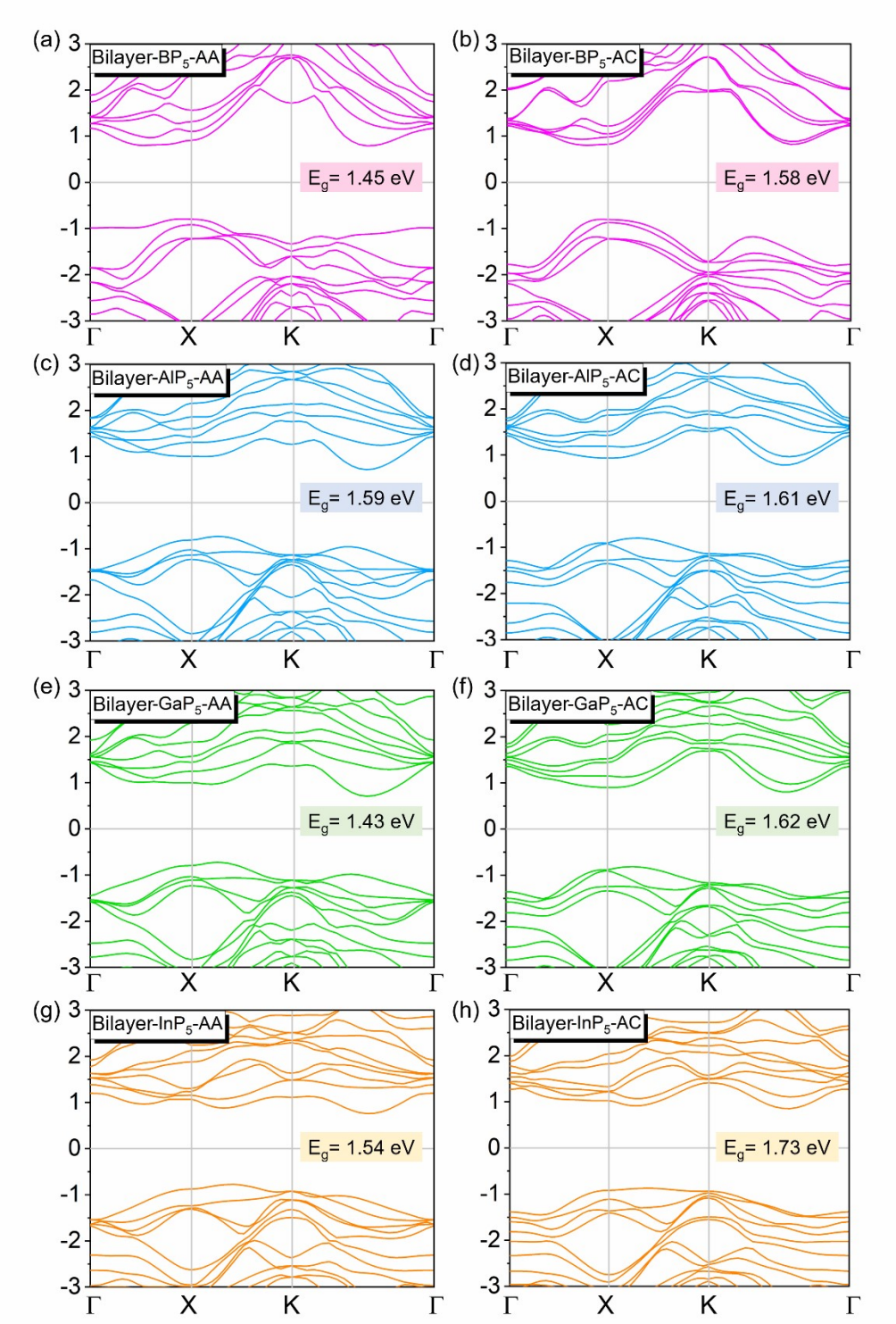

Figure S6. The calculated band structures of bilayer Penta-MP_5 in AA pattern and AC pattern relative to the Fermi level in the first Brillouin zone along the path (Γ-X-K-Γ) by the PBE method.

Optical absorption and utilization of Penta-MP_5 monolayers for water splitting

Computational details for the solar-to-hydrogen (STH) efficiency of Penta-MP_5 monolayers

The STH efficiency is evaluated using the methods proposed by Yang et al[3] defined as the product of the efficiency of light absorption (η_{abs}) and carrier utilization (η_{cu}) is calculated as:

$$\eta_{STH} = \eta_{abs} \times \eta_{cu} \quad \text{(S1)}$$

The efficiency of light absorption is defined as:

$$\eta_{abs} = \frac{\int_{E_g}^{\infty} P(h\omega)\,d(h\omega)}{\int_{0}^{\infty} P(h\omega)\,d(h\omega)} \quad \text{(S2)}$$

where $P(h\omega)$ is the AM1.5G solar energy flux at the photon energy $h\omega$ and $E_g$is the band gap of the photocatalyst. The efficiency of carrier utilization (η_{cu}) is defined as:

$$\eta_{cu} = \frac{\Delta G_{H_2O}\int_{E}^{\infty} \frac{P(h\omega)}{h\omega}\,d(h\omega)}{\int_{E_g}^{\infty} P(h\omega)\,d(h\omega)} \quad \text{(S3)}$$

where ΔG_{H_2O} is the potential difference of 1.23 eV for water splitting and E is the energy of photons that can actually be utilized for water splitting.

$$E = \begin{cases} E_g, (\chi_{H_2} \geq 0.2, \chi_{O_2} \geq 0.6) \\ E_g + 0.2 - \chi_{H_2}, (\chi_{H_2} < 0.2, \chi_{O_2} \geq 0.6) \\ E_g + 0.6 - \chi_{O_2}, (\chi_{H_2} \geq 0.2, \chi_{O_2} < 0.6) \\ E_g + 0.8 - \chi_{H_2} - \chi_{O_2}, (\chi_{H_2} < 0.2, \chi_{O_2} < 0.6) \end{cases} \quad \text{(S4)}$$

Computational details for carrier mobilities of Penta-MP_5 monolayers.

The effective mass m^* indicating in different places (VBM for holes and CBM for electrons) is calculated based on the data about the band structure by the equation: $m^* = \hbar^2\left[\frac{\partial^2 E(k)}{\partial k^2}\right]^{-1}$, where k is the wave vector and $E(k)$ is the energy corresponding to k. The $C_{2d} = [\partial^2 E/\partial\delta^2]/S_0$ and

$E_{2d}^{*} = \partial\Delta E/\partial\delta$ are the in-plane stiffness with the longitudinal strain and the deformation potential as the change of band edges in VBM for holes and CBM for electrons when strains are applied in different directions (*a* and *b*), respectively. And S_0 and ΔE are the area of the equilibrium supercell and the value of CBM (VBM) relative to the vacuum energy, respectively. $\delta = \Delta l/l_0$, and E is the total energy.

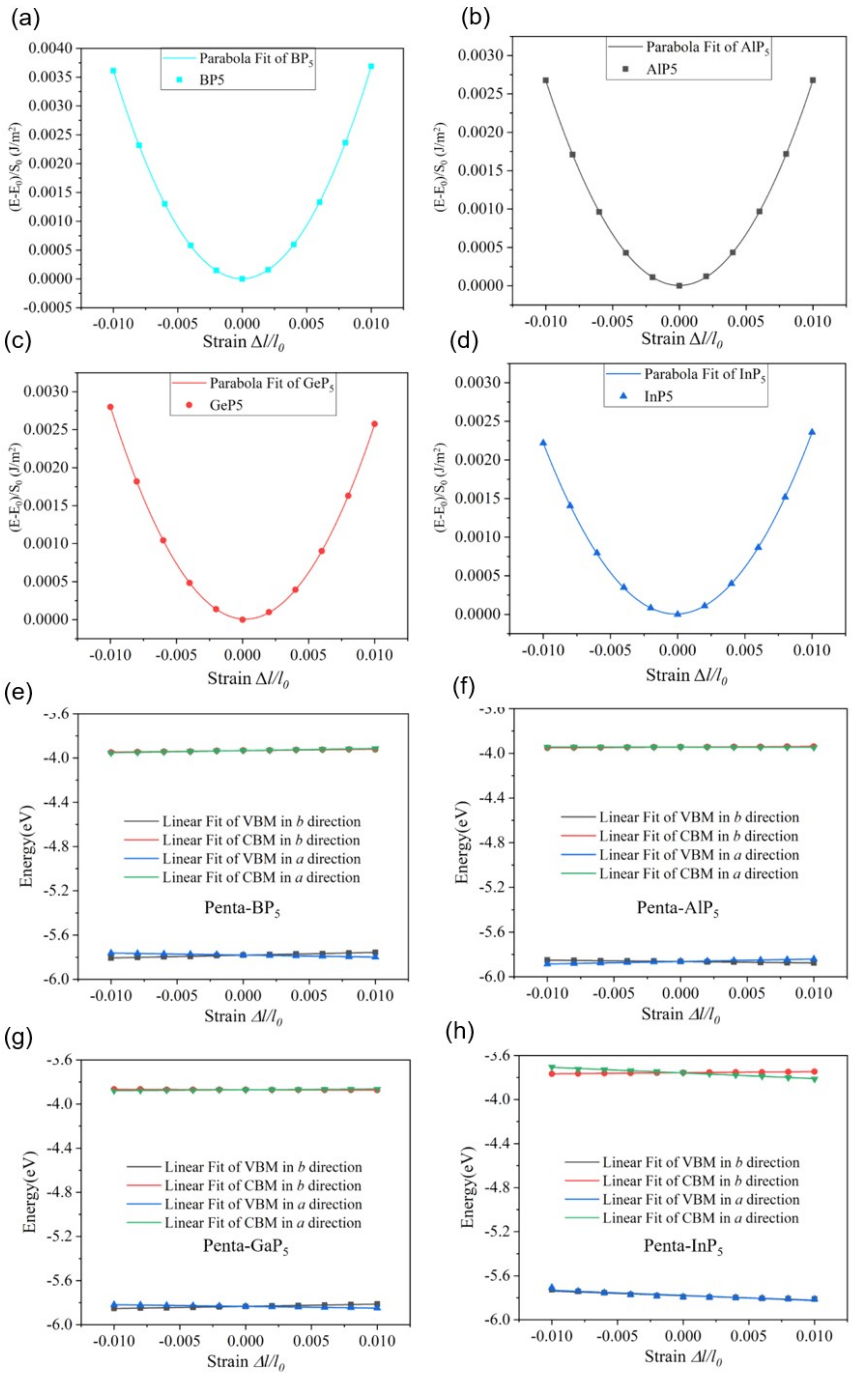

Figure S7. (a-d) The calculated total energy of Penta-MP_5 monolayers in *a* and *b* directions with respect to the strain, respectively. (e-h) The relationship between the shift of VBMs and CBMs with

respect to the vacuum energy and the applied biaxial strain along the *a* and *b* directions of Penta-MP_5 monolayers.

Photocatalytic properties of Penta-MP_5 monolayers for water splitting

Selection of active sites on Penta-MP_5 monolayers

The Penta-MP_5 monolayers are two-dimensional, possessing an infinitely extended atomic surface with thin longitudinal thickness (*z*-direction), the active sites are mainly located on their upper and lower surfaces.[3-6] By analyzing their symmetry, we can find that their upper and lower surfaces are identical. Therefore, we need only consider active sites that may be located on either of the two surfaces (e.g., the upper surface). Meanwhile, in order to avoid the adsorption of intermediates groups (H_2O molecule, -OH, -O and -OOH) leading to excessive distortion of the original structure (Slab), we therefore expanded their unit cells into 2 × 2 × 1 supercells. By studying the adsorption of H_2O molecules on their surfaces (consider four adsorption models with a H_2O adhered in different sites as shown in Figure S8), we find that the H_2O molecules tend to be close to the phosphorus atoms. The adsorption of H_2O molecules is the first step in water-splitting reaction that subsequent reactions are based on. Thus, the phosphorus atom can be tentatively chosen as a possible active site for the water-splitting reaction. Through the structural optimization of the intermediates H*, OH*, O* and OOH* with phosphorus atom as the active site and calculations of the free energy change as shown in Figure 4 and Figure S8, we find that the $\Delta G(H^*)$ for HER are lower than the potential U_e supplied by their photoexcited electrons, and the energy barriers of the OER are lower than the potential U_h supplied by their photoexcited holes. This means that the chosen active site is favorable for the HER reaction and OER reaction, which also verifies our above prediction that phosphorus atom is the active site for the water-splitting reaction.

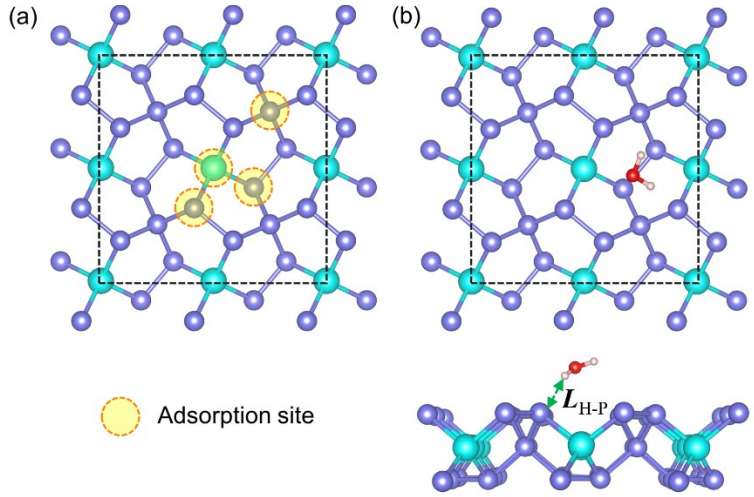

Figure S8. (a)The yellow circles indicate the H_2O molecule adsorption sites on Penta-MP_5 monolayers, (b) the top and side views of the most stable adsorption structures of H_2O on the surface of Penta-MP_5 monolayers. L_{H-P} represents the distance between the oxygen atom of the adsorbed H_2O molecule and its two nearest M atoms.

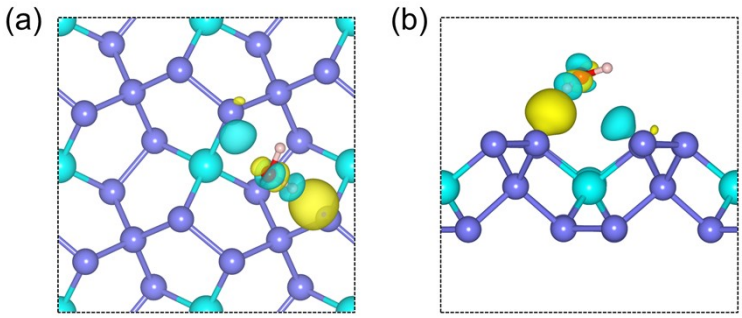

Figure S9. The charge density difference of Penta-MP_5 monolayers top (a) and side(b) views.

Computational details for free energy change of Penta-MP_5 monolayers.

In an aqueous solution, the HER process could be decomposed into two one-electron steps with each step consuming a proton and an electron:

Step (i): $* + H^+ + e^- \rightarrow *H$

Step (ii): $*H + H^+ + e^- \rightarrow * + H_2$

Meanwhile, OER process could be decomposed into four one-electron oxidation steps, corresponding to the deprotonation of water molecules, as follows:

Step 1: $* + H_2O \rightarrow *OH + H^+ + e^-$

Step 2: $*OH \rightarrow *O + H^+ + e^-$

Step 3: $*O + H_2O \rightarrow *OOH + H^+ + e^-$

Step 4: $*OOH \rightarrow * + O_2 + H^+ + e^-$

Where * denotes a site on the surface, *(radical) denotes the corresponding radical adsorbed on the surface. To calculate the free energy changes involved in HER and OER process, Gibbs free energies: $G(T) = E + H(T) - TS(T)$ with E denoting the self-consistent field energy for a given species, can be calculated including all relevant finite temperature contributions to enthalpy $H(T)$ and entropy $S(T)$, i.e. vibration, rotation and translation for gas phase species; for adsorbed species only vibrational contributions were considered since rotational and translational motions become frustrated. Considering the effect of the pH value of solvent and external potential U, the Gibbs free energy changes ΔG are obtained through the following calculations:

$$\Delta G_i = G(*H) - G(*) - \frac{1}{2}G(H_2) + \Delta pH - eU_e$$

$$\Delta G_{ii} = G(*) - G(*H) + \frac{1}{2}G(H_2) + \Delta pH - eU_e$$

$$\Delta G_1 = \frac{1}{2}G(H_2) - G(*OH) - G(*H) - G(H_2O) - \Delta pH - eU_h$$

$$\Delta G_2 = \frac{1}{2}G(H_2) + G(*O) - G(*OH) - \Delta pH - eU_h$$

$$\Delta G_3 = \frac{1}{2}G(H_2) + G(*OOH) - G(H_2O) - \Delta pH - eU_h$$

$$\Delta G_4 = \frac{1}{2}G(H_2) + G(*) - G(*OOH) + G(O_2) - \Delta pH - eU_h$$

Where $G(H^+ + e^-)$ is replaced by $\frac{1}{2}G(H_2)$, considering the reaction of $H^+ + e^- \leftrightarrow \frac{1}{2}H_2$ is in equilibrium state at standard condition (pH = 0, T = 298K, 1atm). $\Delta pH = 0.059 \times pH$ is used to estimate the effect of pH value of solvent. Furthermore, the Gibbs free energy is shifted by the applied oxidation (eU_e) or reduction (eU_h) potential because of the photo-induced electrons or holes. For photocatalytic reactions. U_e and U_h are the potentials for HER and OER, respectively. Herein, the U_e and U_h are the energy difference of CBM and VBM relative to hydrogen reduction potential (H^+/H_2).

Table S5. The calculated Gibbs free energy changes ΔG (eV) of different reaction intermediates in OER on Penta-MP_5 monolayers

Penta-MP_5	pH = 0				pH = 7 (eV)			
	ΔG_1	ΔG_2	ΔG_3	ΔG_4	ΔG_1	ΔG_2	ΔG_3	ΔG_4
Penta-BP_5	1.17	1.13	2.16	0.46	0.76	0.71	1.75	0.05
Penta-AlP_5	1.25	1.63	1.89	0.16	0.84	1.21	1.47	-0.26
Penta-GaP_5	1.26	1.52	1.73	0.41	0.85	1.11	1.32	-0.01
Penta-InP_5	1.20	1.62	1.67	0.43	0.78	1.21	1.26	0.02

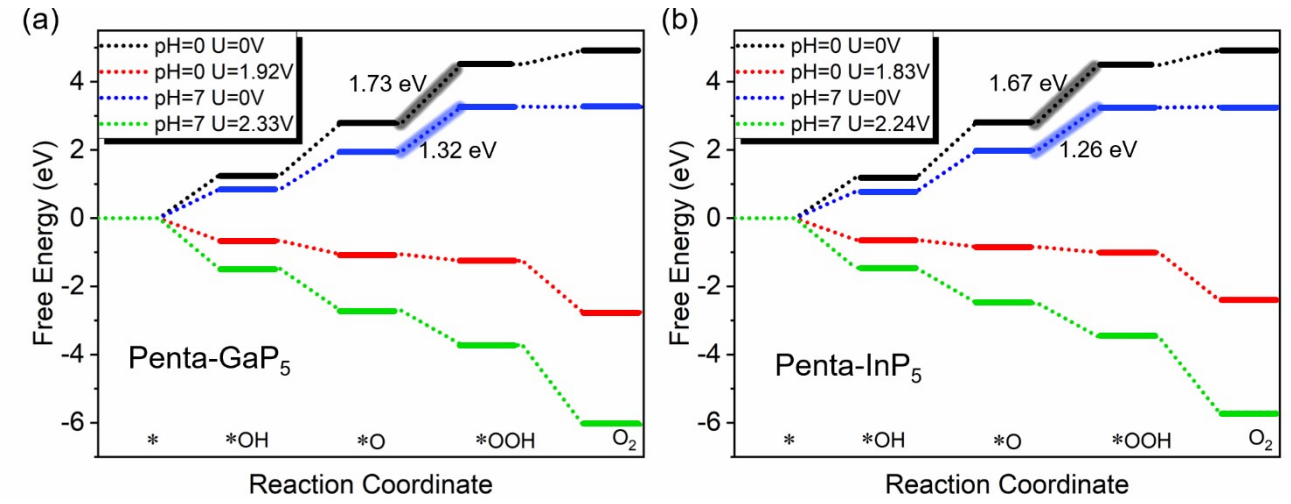

Figure S10. (a)-(b) the calculated Gibbs free energy changes of intermediate states involved in OER processes for Penta-GaP_5 and Penta-InP_5 monolayers at pH = 0 and pH = 7. The short grey and blue broad lines in the diagram indicate the rate-limiting step of the OER without illumination.

References

1. S. Liu, B. Liu, X. Shi, J. Lv, S. Niu, M. Yao, Q. Li, R. Liu, T. Cui and B. Liu, *Scientific Reports*, 2017, **7**, 2404.
2. M. Naseri, *Chemical Physics Letters*, 2018, **706**, 99-106.
3. C.-F. Fu, J. Sun, Q. Luo, X. Li, W. Hu and J. Yang, *Nano Letters*, 2018, **18**, 6312-6317.
4. B. Wei, Z. Fu, D. Legut, T. C. Germann, S. Du, H. Zhang, J. S. Francisco and R. Zhang, *Adv Mater*, 2021, **33**, e2102595.
5. K. Liu, J. Fu, Y. Lin, T. Luo, G. Ni, H. Li, Z. Lin and M. Liu, *Nature Communications*, 2022, **13**, 2075.
6. Q. Xiang and J. Yu, *J. Phys. Chem. Lett.*, 2013, **4**, 753−759.